Selective Spin-State Switch and Metal-Insulator Transition in $GdBaCo_2O_{5.5}$.

C. Frontera[1], J.L. García-Muñoz[1], A. Llobet[2], and M.A.G. Aranda[3]
[1]*Institut de Ciència de Materials de Barcelona, CSIC, Campus de la UAB, E-08193 Bellaterra, Spain.*
[2]*Laboratoire de Magnetisme Louis Néel, CNRS 25 Avenue des Martyrs - BP 166, 38042 Grenoble Cedex 9, France.*
[3]*Departamento de Química Inorgánica, Cristalografía y Mineralogía Universidad de Málaga, 29071 Málaga, Spain.*
(Dated: February 1, 2008)

Ultra-high resolution synchrotron diffraction data for $GdBaCo_2O_{5.5}$ throw new light on the metal-insulator transition of Co^{3+} Ba-cobaltites. An anomalous expansion of CoO_6 octahedra is observed at the phase transition on heating, while CoO_5 pyramids show the normal shrinking at the closing of the gap. The insulator-to-metal transition is attributed to a sudden excitation of some electrons in the octahedra (t_{2g}^6 state) into the Co e_g band (final $t_{2g}^4e_g^2$ state). The $t_{2g}^5e_g^1$ state in the pyramids does not change and the structural study also rules out a $d_{3x^2-r^2}/d_{3y^2-r^2}$ orbital ordering at T_{MI}.

PACS numbers: 71.30.+h,71.38.+i,75.30.Kz

Transition metal oxides with perovskite structure have demonstrated to present a wide variety of challenging phenomena. Superconductivity and colossal magnetoresistance of Cu and Mn oxides are spectacular phenomena related with the strong spin-charge-lattice correlations occurring in these materials. Cobaltites are also very challenging since, in addition, the spin state degree of freedom of Co ions introduces new effects in these narrow band oxides[1,2]. The competition between crystal field (CF), on-site Coulomb correlations and the intra-atomic exchange energies leads to the existence of three possible spin states of Co^{3+} ions: the low spin state (LS, $t_{2g}^6e_g^0$), the intermediate spin state (IS, $t_{2g}^5e_g^1$), and the high spin state (HS, $t_{2g}^4e_g^2$). HS (LS) is associated with small (high) values of CF (when compared with the intra-atomic exchange energy). The IS state appears when similar values of these two energies are combined with the electron-phonon coupling and the Jahn-Teller distortion that lifts the degeneracy of e_g and t_{2g} orbitals. In many cobaltites the energy differences between spin states are small and can be easily overcome by thermal fluctuations and/or changed by the lattice thermal evolution[2] leading to spin state transitions.

More recently, a great interest on $LnBaCo_2O_{5+\delta}$ (Ln ≡ Rare earth) cobaltites has appeared[3,4,5,6,7,8,9,10]. This family of compounds presents very interesting phenomena like spin state transitions[6,9,10], charge ordering[7,8], and giant magnetoresistance[4,10]. The oxygen content δ ($0 \leq \delta \leq 1$) controls the nominal valence of Co ions that varies from 3.5+ (50% of Co^{3+} and 50% of Co^{4+}) for $\delta = 1$ to 2.5+ (50% of Co^{3+} and 50% of Co^{2+}) for $\delta = 0$ passing through 100% of Co^{3+} for $\delta = 0.5$. The oxygen vacancies introduced when $\delta < 1$ are found to be placed in layers together with the rare earth ions. Thus, these compounds are formed by the stacking sequence $[CoO_2][BaO][CoO_2][LnO_\delta]$ along the c direction, and Co presents coexistence of two types of coordination environments: pyramidal CoO_5 and octahedral CoO_6. Moreover, oxygen vacancies, within the $[LnO_\delta]$ layers, present a remarkably strong tendency to order. This tendency prevents the appearance of disorder in the magnetic superexchange interactions, which causes spin glass behavior in oxygen deficient $La_{1-x}Sr_xCoO_{3-\epsilon}$ compounds. For $\delta = 0.5$ the oxygen atoms and vacancies are located in alternating rows[5,9]. A HS state has been attributed to Co^{3+} in pyramidal environment (a rather unusual coordination) from neutron data in $HoBaCo_2O_5$ (exclusively pyramidal $Pmma$ structure)[8]. In contrast, for pseudocubic $LaCoO_3$, a large cubic-CF splitting stabilizes, at low temperature, the LS configuration[12] while at high temperature the coexistence of HS and IS state has been reported[2]. LS has been proposed for $LaBaCo_2O_6$ (octahedral environment) at low temperature[6]. Here we should note that the deformation of the pyramid in $\delta = 0$ $Pmma$ cobaltites with small lanthanides[7,8] is meaningfully different to that observed in $\delta = 0.5$ cobaltites and intermediate Ln^{3+} size[9], so that the differences in the CF splitting may give rise to different electronic configurations. Namely, the same type of coordination environment may hold different spin states depending on the lattice deformation and/or orbital occupancy[12].

Several $LnBaCo_2O_{5.5}$ compounds present a metal-insulator (MI) transition at a temperature (T_{MI}) ranging between 280 and 400 K (depending on Ln). Susceptibility measurements reveal that coinciding with this transition there is a large change in the effective paramagnetic moment of the samples. This is understood as a sudden increase, on heating, in the spin state of Co ions[5,9,10]. From magnetic measurements on several samples with different lanthanides, all displaying the MI transition, Maignan *et al.*[5] suggested a coexistence of IS (pyramids) and LS (octahedra) for $T < T_{MI}$ and HS Co^{3+} at high enough temperatures. Nevertheless, the spin state at both sides of the MI transition is still unclear. A study of the structural changes was carried out for $TbBaCo_2O_{5.5}$ by Moritomo *et al.*[9]. Based on these structural data, they proposed a spin state transition from a full IS state scheme to the HS state (for Ln=Tb) in both pyramidal and octahedral sites[9]. For $T > T_{MI}$ a HS state[5,9] and a coexistence of HS/IS states have been proposed[10] by different groups. The main conclusion of Moritomo *et al.* is that the orbital degree of freedom of the IS state ($t_{2g}^5e_g^1$) and the electron-phonon coupling results in a Jahn-Teller cooperative distortion and a $d_{3x^2-r^2}/d_{3y^2-r^2}$ type orbital

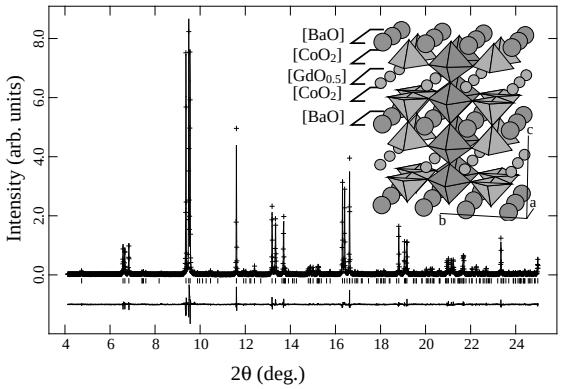

FIG. 1: Observed (crosses), calculated and difference SXRPD patterns for $GdBaCo_3O_{5.5}$ at 340 K ($\lambda = 0.45029$ Å). The compound is orthorhombic ($P\,mmm$; Z=2) with $a_p \times 2a_p \times 2a_p$ perovskite superstructure. The inset shows a polyhedral view of the orthorhombic perovskite structure of $GdBaCo_2O_{5.5}$ (large circles are Ba^{2+} cations and small circles are Gd^{3+} cations).

order (OO) below T_{MI}. As the origin of the transition they proposed a sudden distortion of the basal planes, on cooling, that accommodate the $d_{3x^2-r^2}$ (pyramid) and $d_{3y^2-r^2}$ (octahedron) orbital occupancy[9]. However, the sample studied in Ref. 9 had impurities and the reported errors in the Co-O distances were anomalously large.

In this paper, we describe striking structural features for $GdBaCo_2O_{5.5}$ across T_{MI}. Interatomic Co-O distances exhibit a very different evolution in octahedra and pyramids. Analysis of diffraction and magnetic data through the insulator-to-metal transition provide evidence for a low-to-high spin transition only in octahedra. The Q_2-type distortion of the basal plane of octahedra and pyramids do not increase below T_{MI} ruling out a $d_{3x^2-r^2}/d_{3y^2-r^2}$ orbital ordering as the driving force for the phase transition. The metallic phase is caused by excitation of electrons, from Co atoms placed at the CoO_6 octahedra, into the e_g band.

$GdBaCo_2O_{5+\delta}$ was prepared by standard solid-state reaction in air at $T = 1125^oC$ during 24 h. After regrinding of the pellet, the compression and annealing processes were repeated several times. As Gd has a very high neutron absorption coefficient, we have characterized the structural evolution across the MI transition using X-ray thermodiffractometry. Ultra-high resolution synchrotron X-ray powder diffraction (SXRPD) patterns were collected at BM16 diffractometer of ESRF (Grenoble) in the standard Debye-Scherrer configuration. The polycrystalline sample was loaded in a borosilicate glass capillary ($\phi = 0.5$ mm) and rotated during data collection. A short wavelength, $\lambda = 0.450294(6)$ Å (27.54 keV), selected with a double-crystal Si (1 1 1) monochromator, and calibrated with Si NIST ($a = 5.43094$ Å), was chosen to reduce the sample absorption. Measurements have been done at T= 300, 320, 340, 360, 380 and 400 K. Each SXRPD run took about $\frac{3}{4}$ h to have good statistics over the angular range $4^o \leq 2\theta \leq 25^o$ with 0.005^o step size. The powder patterns were analyzed by the Rietveld method using the GSAS suite of programs[11]. No impurities peaks have been detected and the diffraction peaks were remarkably sharp for a three metal-containing perovskite. The oxygen stoichiometry was determined to be 5.53(1) from SXRPD data, an usual oxygen content found for air-synthesis[5,9]. Moreover, according to Ref. 5 the MI transition in absent in Gd samples with $\delta \geq 0.6$. Characterization of the sample included magnetic measurements (SQUID) in the temperature range $10\,K \leq T \leq 650\,K$. Magnetotransport, magnetic and optical transmission measurements under pulsed fields up to 35 T have been also carried out[10].

First, we want to focus on the crystal structure and the ordering of the oxygen vacancies. The structure of $TbBaCo_2O_{5.5}$ reported in Ref. 9 was used as starting model for the Rietveld refinements. We will use the same atomic labelling scheme for the sake of comparison. In the crystal structure ($P\,mmm$) the simple perovskite cell is doubled along the b-axis in order to account for alternating oxygen rich and oxygen deficient $a-c$ layers. The oxygen vacancies were checked in our $GdBaCo_2O_{5.5}$ sample and found to be located at the lanthanide layers. O3' at $(0,0,\frac{1}{2})$ is almost empty with a refined occupation factor of 0.08(2). O3 at $(0,\frac{1}{2},\frac{1}{2})$ is fully occupied with a refined occupation factor of 0.99(2). So, there are octahedra chains along the c-axis alternated along the b-axis with the corner-sharing square pyramids in both cobaltites. Figure 1 shows the SXRPD Rietveld plot at 340 K as an example. Refined atomic coordinates and agreement factors are given in Tab. I. The crystal structure of $GdBaCo_2O_{5.5}$ is shown in the inset of Fig. 1. From this structure it is apparent that the metallic phase should be highly anisotropic. Oxygen vacancies preclude the existence of highly conducting paths along c within the $a-c$ layers of pyramids.

On cooling through the transition, b and c lattice parameters exhibit a sudden shrink (0.28% and 0.27%, respectively) while a lengthens at T_{MI} (0.35%), see Fig. 2(a). The values found, and their thermal evolution, strongly contrast with those reported in Ref. 9 for $TbBaCo_2O_{5.5}$, where $a > b/2$, a shrinks (on cooling) at T_{MI} and $b/2$ lengthens. Figures 2(b) and 2(c) show the Co-O bond distances, for $Co1O_6$ octahedron and $Co2O_5$ pyramid respectively, along the three crystallographic axes (Co-Oi stands for the lengths along i=a, b and c axes) derived from the refined atomic coordinates given in Tab. I. Again, there are important differences with the case of $TbBaCo_2O_{5.5}$. We have found that pyramids and octahedra are deformed in both the insulating and metallic states. The longest Co-O distance is Co-Oa for the former ($Co2O_5$) and Co-Ob for the latter ($Co1O_6$). Long and short bonds alternate along the b axis at both sides of the transition. A pattern well different to the evolution proposed in Ref. 9 for $TbBaCo_2O_{5.5}$, where that alternation was only clearly observed below T_{MI}, proposing that the basal plane deformation in pyramids and octahedra

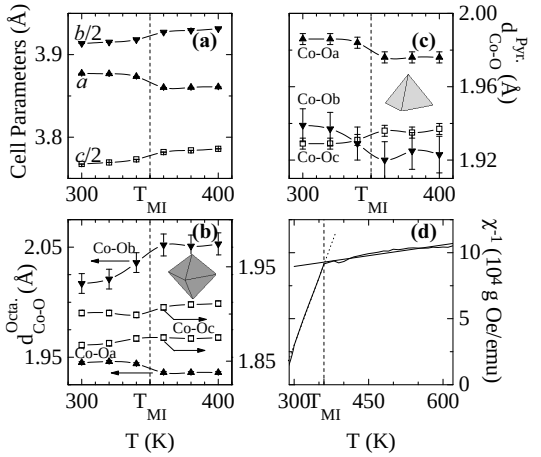

FIG. 2: Temperature dependence of **(a)** lattice constants; **(b)** Co-O bond distances for the CoO_6 octahedra (Co-Oi stands for the bond lengths along i=a, b and c axes); **(c)** Co-Oi bond distances for the CoO_5 pyramids; and **(d)** inverse of the susceptibility $\chi_{\rm Co}$ (the straight lines show the Curie fits above and below T_{MI}.

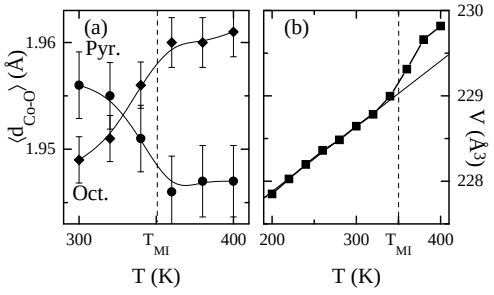

FIG. 3: Temperature dependence of **(a)** average Co-O distances for the CoO_6 and CoO_5 polyhedra and **(b)** unite cell volume. The continuous straight line in **(b)** is a guide-to-the-eyes to highlight the anomalous volume expansion at T_{MI}.

vanishes above T_{MI}. Hence, conversely with Ref. 9, our data discard the stabilization of a $d_{3x^2-r^2}/d_{3y^2-r^2}$-type orbital ordering below T_{MI} as the physical mechanism for the MI transition in $GdBaCo_2O_{5.5}$. Furthermore, we show in Figs. 2(b) and 2(c) that the difference between long and short Co-O bonds in the basal plane (the Q_2-type antiferrodistorsive distortion) remains practically unchanged in the pyramid (0.06 Å) but increases strongly in the octahedron when heating above T_{MI}. This evolution clearly rules out the aforementioned orbital order transition.

Fig. 2(d) shows the temperature dependence of the inverse susceptibility (measured in a field of 1 T after a zero field cooling process) in the paramagnetic region up to 625 K. The paramagnetic contribution from Gd atoms (estimated between 10-625 K, $\chi_{\rm Gd} = \dfrac{1.92 \cdot 10^{-2}}{T + 0.4} \dfrac{emu}{g\,Oe}$) was subtracted in order to extract the contribution coming only from Co ions [$\chi_{\rm Co} = 1/2(\chi - \chi_{\rm Gd})$]. A drastic change in the effective moment $\mu_{\rm eff}$ and the sign of the Curie temperature takes place coinciding with the electronic localization. According to the Curie-Weiss fitting shown in Fig. 2(d) $\mu^{\rm Co}_{\rm eff}$ per Co atom changes from $\mu^{\rm Co}_{\rm eff} = 1.8(1)\,\mu_{\rm B}$ ($T < T_{MI}$) to $4.3(2)\,\mu_{\rm B}$ ($T > T_{MI}$). The expected values for Co^{3+} full IS, 1:1 mixture LS/IS, IS/HS or full HS are respectively 2.83, 2.00, 4.00 and 4.90 $\mu_{\rm B}$. The possibility of a non-negligible orbital contribution to the moment in this compound is uncertain[13]. However, below T_{MI} (in the paramagnetic insulating phase) the effective moment found per Co atom agrees with a 1:1 mixture of Co^{3+} in LS and IS, ruling out the full Co^{3+} IS scheme. Since IS Co^{3+} is most probable in the pyramids[5,13], the results indicate that, below T_{MI}, the octahedron contains LS Co^{3+} and the pyramid IS Co^{3+}. Interestingly, the moment per Co atom deduced in the metallic phase below 625 K agrees with a half of Co^{3+} ions in IS and the other half in HS states.

Before discussing the most probable scenario for the metal-insulator transition, let us analyze in more detail the Co-O bond length variation. Does that structural evolution corroborate the picture deduced from magnetic data? The answer is positive. As shown in Fig. 2(c), Co-Oa and Co-Ob basal distances of the pyramid both lengthen on cooling, in a so similar way that the basal plane deformation remains practically unchanged at both sides of T_{MI}. Moreover, the apical Co-Oc distance of the pyramid changes little across the transition. We want to emphasize that these changes are very different to those observed in the octahedron. They are shown in Fig. 2(b) and Fig. 3(a): the Co-Ob distance in the octahedra displays a pronounced shrinking on cooling, which is accompanied by a moderate increase of the Co-Oa distance (again the Co-Oc apical distances change little). As a result, in contrast with the pyramid, the difference between the two diagonal distances of the octahedra increases notably when enters the metallic phase. At this point it is important to recall that a transition to a higher spin-state in Co^{3+} (as deduced from magnetic data) implies a bigger effective ionic radius which should lengthen the average $\langle d_{\rm Co-O} \rangle$ bond length. Hence, a very significant finding is the different evolution of the average $\langle d_{\rm Co-O} \rangle$ distance in the octahedron and the pyramid [Fig. 3(a)]. So, a central result is that the average $\langle d_{\rm Co-O} \rangle$ distance of the octahedron increases substantially at T_{MI} on heating. This finding constitutes the first experimental result establishing that the spin-state transition in $LnBaCo_2O_{5.5}$ occurs solely in the octahedra. Thus, in the pyramids we observe, on heating, the metal-oxygen bond-length contraction normally found when the gap closes and enters the metallic phase, indicating again that the transition to a higher spin-state detected in the susceptibility takes place in the octahedron, but not in the pyramid. This transition is also responsible for the anomalous volume expansion at T_{MI} plotted in Fig. 3(b). Normally, the cell volume contracts in an electron delocalization process. The volume expansion observed here is another confirmation of the transition to a higher spin-state.

TABLE I: Atomic positions for $GdBaCo_2O_{5.53(1)}$ from synchrotron powder diffraction Rietveld refinements. The sites are Ba 2o $(\frac{1}{2}, y, 0)$; Gd 2p $(\frac{1}{2}, y, \frac{1}{2})$; Co1 2r $(0, \frac{1}{2}, z)$; Co2 2q $(0, 0, z)$; O1 1a $(0, 0, 0)$; O2 1e $(0, \frac{1}{2}, 0)$; O3 1g $(0, \frac{1}{2}, \frac{1}{2})$;O3' 1c $(0, 0, \frac{1}{2})$ [occupation factor= 0.08(2)]; O4 2s $(\frac{1}{2}, 0, z)$; O5 2t $(\frac{1}{2}, \frac{1}{2}, z)$; O6 4u $(0, y, z)$.

$T(K)$	Ba(y)	Gd(y)	Co1(z)	Co2(z)	O4(z)	O5(z)	O6(y)	O6(z)	R_F (%)
300	0.2500(2)	0.2722(2)	0.2522(5)	0.2561(4)	0.3132(16)	0.2737(18)	0.2450(12)	0.2929(11)	3.91
320	0.2500(2)	0.2718(2)	0.2521(5)	0.2559(4)	0.3134(16)	0.2745(18)	0.2449(12)	0.2925(11)	3.77
340	0.2496(2)	0.2708(2)	0.2517(5)	0.2558(4)	0.3131(15)	0.2744(17)	0.2434(11)	0.2940(10)	3.80
360	0.2493(2)	0.2686(2)	0.2521(5)	0.2560(5)	0.3119(16)	0.2723(18)	0.2418(12)	0.2936(10)	4.20
380	0.2492(2)	0.2685(2)	0.2524(5)	0.2557(5)	0.3115(16)	0.2720(18)	0.2421(12)	0.2939(10)	4.02
400	0.2493(2)	0.2683(2)	0.2524(5)	0.2558(5)	0.3116(16)	0.2723(18)	0.2419(12)	0.2934(10)	4.36

Recapitulating, the analysis of the structural changes and susceptibility data for $GdBaCo_2O_{5.5}$ has permitted to draw a detailed picture of the metal-insulator transition in the $LnBaCo_2O_{5.5}$ family of compounds. Our results reveal that: (i) There is a sudden expansion of the average $\langle d_{Co-O} \rangle^{octa}$ distance at T_{MI}, concomitant with a spin-state transition from LS (insulating) to HS (metallic) state in the Co^{3+} ions of the octahedra. (ii) Co atoms in the pyramids hold the same spin-state (Co^{3+} IS) before and after the electronic delocalization. Hence, the pyramid simply shrinks as commonly observed in Mott oxides when enters the metallic phase. (iii) These findings imply the existence of spin state ordering below and above T_{MI}. (iv) The alternation of short and long Co-O bonds along the b axis is present in the insulating and the metallic phases (and not only in the former, as reported in Ref. 9 for $TbBaCo_2O_{5.5}$). The Q_2-type distortion (antiferrodistorsive) of the basal planes does not increase in the insulating phase, ruling out a $d_{3x^2-r^2}/d_{3y^2-r2}$ type orbital ordering as the origin of the transition. To conclude, the driving force for the MI transition is a spin-state switch in the Co^{3+} ions located at the octahedra. They suddenly switch from LS ($t_{2g}^6 e_g^0$) to HS ($t_{2g}^4 e_g^2$) state at T_{MI}. Thereby, the metallic conductivity in this family of oxides (full Co^{3+}) seems related with the injection of electrons in the conduction band that accompanies the stabilization of a HS ($t_{2g}^4 e_g^2$) state in the CoO_6 octahedra.

Financial support by the MEC (PB97-1175), CICyT (MAT97-0699, MAT97-326-C4-4, and MAT99-0984-C03-01) and Generalitat de Catalunya (GRQ95-8029) projects is thanked. ESRF is acknowledged for the provision of X-ray synchrotron facilities and Dr. E. Dooryee for his assistance during data collection.

[1] G. Thornton, B.C. Tofield and A.W. Hewat, J. Solid State Chemistry **61**, 301 (1986). M.A. Señaris-Rodríguez and J.B. Goodenough, J. Solid State Chem. **116**, 224 (1995). W.C. Koehler and E.O. Wollan, J. Phys. Chem. Solids **2**, 100 (1957). J.B. Goodenough, J. Phys. Chem. Solids **6**, 287 (1958). M. Zhuang, W. Zhang, and N. Ming, Phys. Rev. B **57**, 10705 (1998). T. Saitoh, T. Mizokawa, A. Fujimori, M. Abbate, Y. Takeda, and M. Takano, Phys. Rev. B **55**, 4257 (1997). S. Yamaguchi, Y. Okimoto, and Y. Tokura, Phys. Rev. B **55**, R8666 (1997). M.A. Korotin, S.Yu. Ezhov, I.V. Solovyev, V.I. Anisimov, D.I. Khomskii, and G.A. Sawatski, Phys. Rev. B **54**, 5309 (1996).

[2] K. Asai, A. Yoneda, O. Yokokura, J.M. Tranquada, G. Shirane and K. Kohn, J. Phys. Soc. Jpn. **67**, 290 (1998).

[3] W. Zhoug, C.T. Lin, and W.Y. Liang, Adv. Mater. **5**, 735 (1993). W. Zhou, Chem. Mater. **6**, 441 (1994). C. Martin, A. Maignan, D. Pelloquin, N. Nguyen, B. Raveau, Appl. Phys. Lett. **71**, 1421 (1997). Y. Moritomo, M. Takeo, X.J. Liu, T. Akimoto, A. Nakamura, Phys. Rev. B **58**, R13334 (1998).

[4] I.O. Troyanchuk, N.V. Kasper, D.D. Khalyavin, H. Szymczak, R. Symczak, M. Baran, Phys. Rev. Lett. **80**, 3380 (1998); Phys. Rev. B **58**, 2418 (1998).

[5] A. Maignan, C. Martin, D. Pelloquin, N. Nguyen, B. Raveau, J. Sol. State Chem. **142**, 247 (1999).

[6] E. Suard, F. Fauth, V. Caignaert, Physica B **276-278**, 254 (2000).

[7] T. Vogt, P.M. Woodward, P. Karen, B.A. Hunter, P. Henning, A.R. Moodenbaugh, Phys. Rev. Lett. **84**, 2969 (2000).

[8] E. Suard, F. Fauth, V. Caignaert, I. Mirebeau, G. Baldinozzi, Phys. Rev. B **61**, R11871 (2000).

[9] Y. Moritomo, T. Akimoto, M. Takeo, A. Machida, E. Nishibori, M. Takata M. Sakata, K. Ohoyama, A. Nakamura, Phys. Rev. B **61**, R13325 (2000).

[10] M. Respaud, C. Frontera, J.L. García-Muñoz, M.A.G. Aranda, B. Raquet, J.M. Broto, H. Rakoto, M. Goiran, A. Llobet, and J. Rodríguez-Carvajal, Phys. Rev. B **64**, 214401 (2001).

[11] A.C. Larson, and R.B. Von Dreele, Los Alamos National Lab. Rep. No. LA-UR-86-748 (1994).

[12] H. Wu, Phys. Rev. B **62**, R11953 (2000).

[13] S.K. Kwon, J.H. Park, and B.I. Min, Phys. Rev. B **62**, R14637 (2000).